ScienceAdvances
AAAS

advances.sciencemag.org/cgi/content/full/3/12/e1701629/DC1

Supplementary Materials for

Skin-like biosensor system via electrochemical channels for noninvasive blood glucose monitoring

Yihao Chen, Siyuan Lu, Shasha Zhang, Yan Li, Zhe Qu, Ying Chen, Bingwei Lu, Xinyan Wang, Xue Feng

Published 20 December 2017, *Sci. Adv.* **3**, e1701629 (2017)
DOI: 10.1126/sciadv.1701629

The PDF file includes:

- fig. S18. Skin surface condition.
- Legend for movie S1

Other Supplementary Material for this manuscript includes the following:
(available at advances.sciencemag.org/cgi/content/full/3/12/e1701629/DC1)

- movie S1 (.mp4 format). ROSE transfer printing.

Supplementary Text

Theoretical analysis of the HA's effect in the ETC

In the reverse iontophoresis, two major transport mechanisms are involved: electromigration and electroosmosis.

Electromigration is the movement of small ions across the skin under the direct influence of an electric filed. Electron fluxes are transformed into ionic fluxes by the electrode reactions, and ionic transport proceeds through the skin to maintain electroneutrality. The total charge transported depends on the strength of the electric filed and the duration of application. Iontophoresis sets in motion several ions across the skin, and all of them compete to carry a fraction of the current. The contribution of each ion to charge transport is called the transport number, the sum of which equals 1. According to Faraday's law, the flux of each ion in the iontophoretic circuit is given by

$$J_i = \frac{t_i \times I}{F \times z_i} \tag{1}$$

where J_i is the flux of the *i*th ion, t_i is its transport number, and z_i is the valence; F is Faraday's constant; and I is the total current. Transport numbers depend on the relative mobilities and concentrations of all mobile ions in the iontophoretic system and, given that NaCl is the principal extracellular electrolyte in the body, Na^+ and Cl^- carry a major fraction of the current in iontophoresis and reverse iontophoresis.

Electroosmosis is the principal transport mechanism of uncharged molecules (such as glucose) and of high-molecular-weight cations. The electroosmosis dominates the transport of the glucose through the skin. The skin is negatively charged at physiologic pH and acts, therefore, as a permselective membrane to cations. This preferential passage of counterions induces an electroosmotic solvent flow that may carry neutral molecules in the anode-to-cathode direction. The volume flow, J_v [volume/(time·area)] is predicted to be proportional to the potential gradient ($-\mathrm{d}\phi/\mathrm{dx}$) established by the electric filed

$$J_v = L_{ve}\left(\frac{-d\phi}{dx}\right) \tag{2}$$

where L_{ve} is the electroosmotic flow coefficient describing the direction and the magnitude of the volume flow. The molar flux of a solute *j* present at a molar concentration c_j is then

$$J_j = J_v \times c_j \tag{3}$$

Combine equation (2) and equation (3) we can get the computational formula of the molar flux of a solute such as glucose as

$$J_j = L_{ve}\left(\frac{-d\phi}{dx}\right) \times c_j \tag{4}$$

According to equation (4), the molar flux of the solute (in this case, glucose) is not only determined by the potential gradient across the skin but also the molar concentration of the initial solute (i.e. the glucose density in the ISF).

In our experiments, when the HA is penetrated into the subcutaneous tissue, the HA also acts as the moisturizer. The HA's ability to hold water increases the water content of the skin. According to the previous research [8], the skin water content is proportional to $\frac{1}{R}$ where R is the skin impedance. According to experiment result of the HA's influence on the skin water content, after spraying HA (concentration 0.1%) for 1h, the skin water content rises from ~30% to ~43% so the water content rising ratio WCRR is

$$\text{WCRR} = \frac{43\%}{30\%} = 1.43(\text{for young people})$$

Based on the proportional relationship between skin impedance and skin water content, the skin impedance after spraying HA will decrease.

In the electrochemical twin channels system, the total skin impendences of the anode channel R_a and the cathode channel R_c can be simplified as series connection of two equal impendences. So, the total skin impedance before spraying HA is

$$R_{before} = R_a + R_c = 2R$$

The HA decreases the R_a so that the after-HA-spray total impedance is

$$R_{after} = R_{a'} + R_{c'} = \frac{1}{WCRR} R_a + R_c = 1.7R = 0.85R_{before}$$

The solute flux outward the skin exists through the cathode channel so the potential gradient from the ISF to the cathode is responsible for the flux. As the R_a and R_c are series-connected, the potential gradient of the cathode channel after spraying HA $\nabla\phi_a$ is

$$\nabla\phi_a = \frac{d\phi}{dx} = \frac{U}{R_{after}} \times R_c = \frac{U}{0.85R_{before}} \times R_c = 1.18\left(\frac{U}{R_{before}} \times R_c\right) = 1.18\nabla\phi_b$$

where $\nabla\phi_b$ is the potential gradient of the cathode channel before spraying HA.
In Fig. 4C, the device response of the reverse iontophoresis without HA penetration is about 6.35 nA/cm^2, and the response with HA penetration is about 107.05 nA/cm^2, which is 16.86 times higher. The moisturizer-induced potential gradient rise (1.18 times) is not enough to yield such response increase. According to equation (4), the molar concentration of the glucose in the ISF must have increased because of the ETC-induced intravascular glucose re-filtration. The estimated molar concentration rise is

$$\frac{c_{after}}{c_{before}} = \frac{16.86}{1.18} = 14.30$$

In summary, the theoretical analysis proves that the ETC induces more glucose from the blood re-filtrating into the ISF, resulting in more glucose to be extracted to the skin and higher device response.

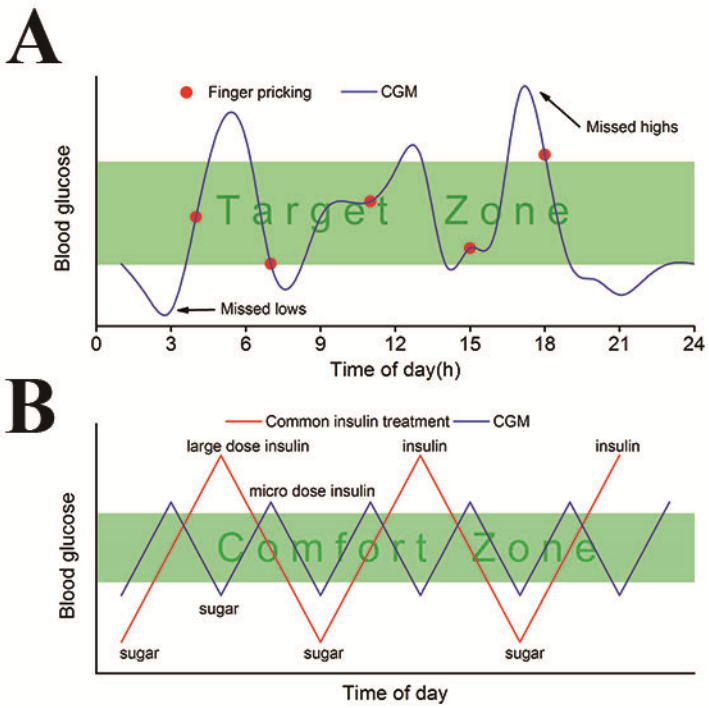

fig. S1. Advantage of CGM over prevalent glucose monitoring and treatment. (**A**) Comparison between CGM and limited times monitoring with finger-pricking glucometer. (**B**) Comparison between CGM with micro insulin pump and common glucose monitoring with insulin treatment

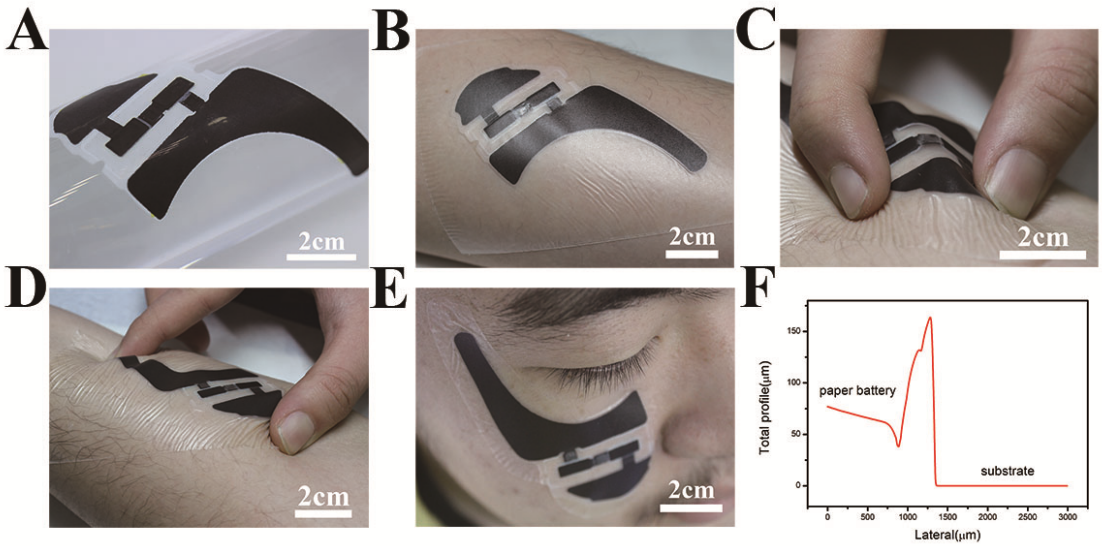

fig. S2. Thin and flexible biocompatible paper battery. (**A**) Paper battery wrapped around a glass rod. (**B**) Paper battery attached to the skin surface. (**C**) The cathode of the paper battery being bended on the skin. (**D**) The paper battery keeping conformal to the skin while being compressed and twisted. (**E**) The paper battery conforms to the face surface, potential for ocular blood glucose measuring. (**F**) Thickness measuring result of the paper battery.

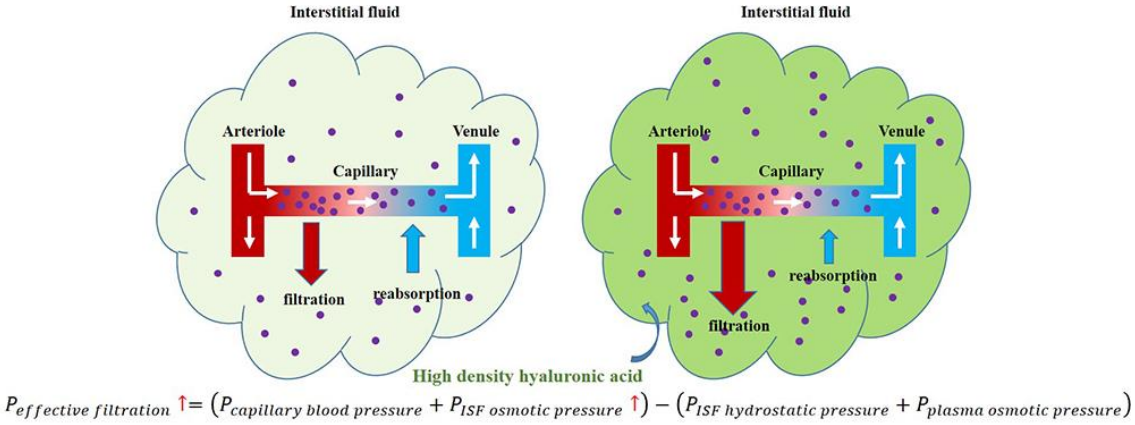

fig. S3. Schematic of high-density HA penetration promoting filtration of glucose in the blood.

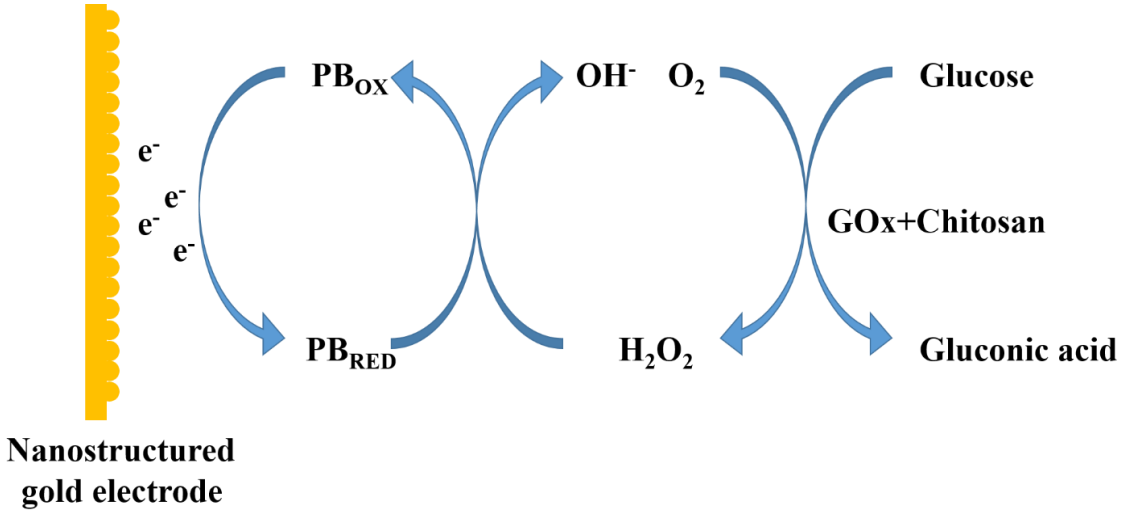

fig. S4. Glucose biosensing principle.

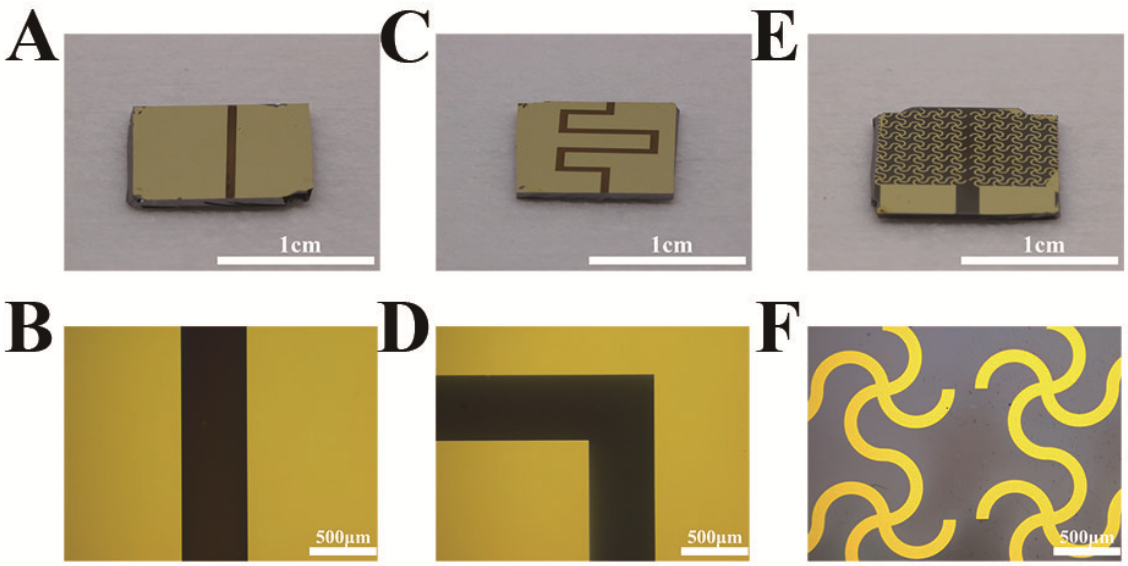

fig. S5. Different patterns for glucose biosensing dual electrode. (**A**) Rectangle electrode. (**B**) Interdigital electrode. (**C**) Serpentine electrode.

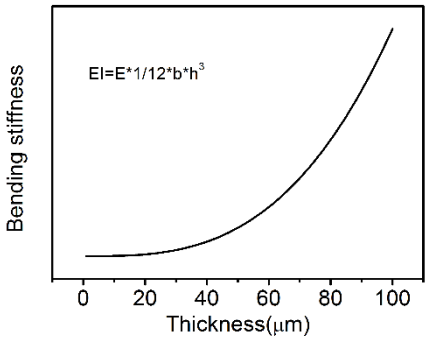

fig. S6. Bending stiffness (that is, flexibility) as a function of device thickness.

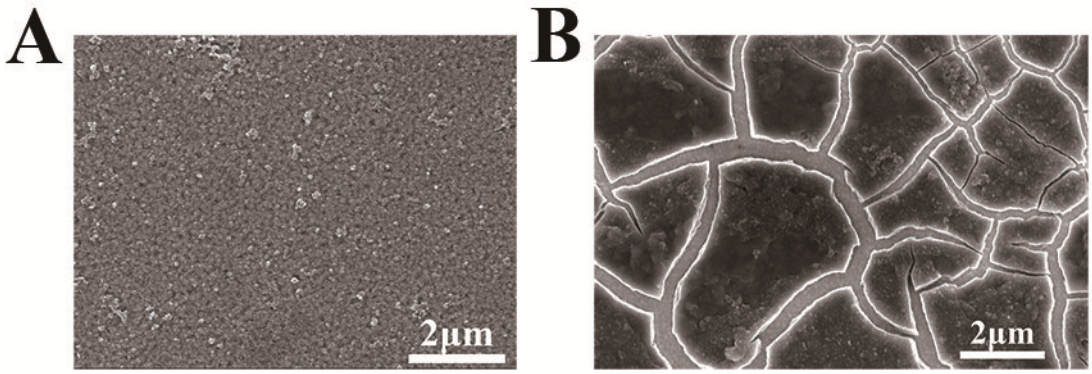

fig. S7. SEM micrographs of electrochemical deposited PB on different gold electrodes. SEM micrographs of (**A**) complete N-PB and (**B**) cracked O-PB.

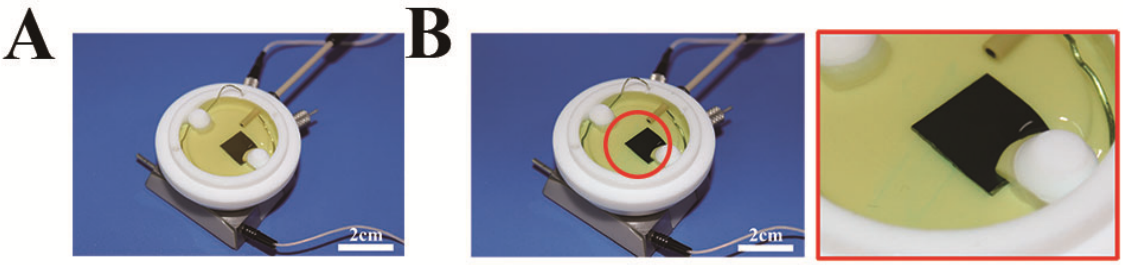

fig. S8. PB sediments after the ECD of O-PB that are not attached to the electrodes. (**A**) Before ECD. (**B**) After ECD (PB sediments shown in red circle)

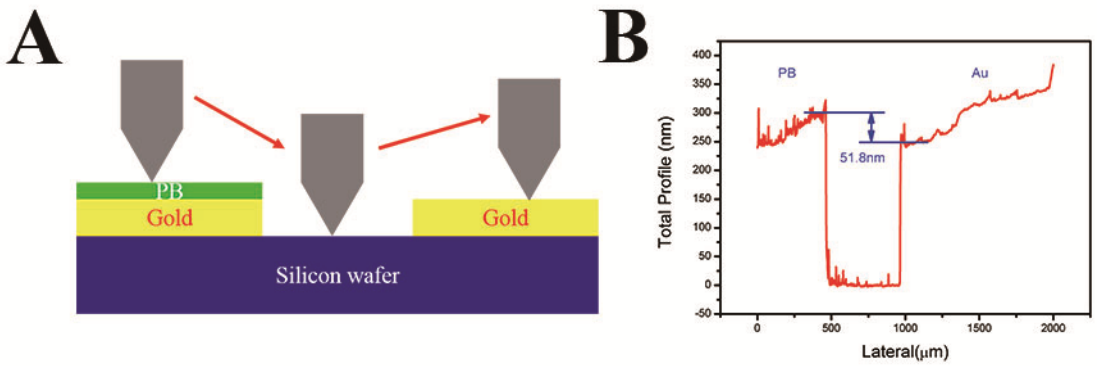

fig. S9. PB thickness measurement. (**A**) Schematic of thickness measurement of N-PB. (**B**) Thickness measuring result.

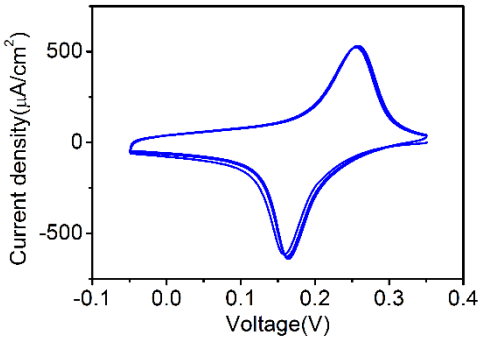

fig. S10. Twenty times of CV scan (−0.05 to 0.35 V versus reference electrode at a scan rate of 50 mV/s).

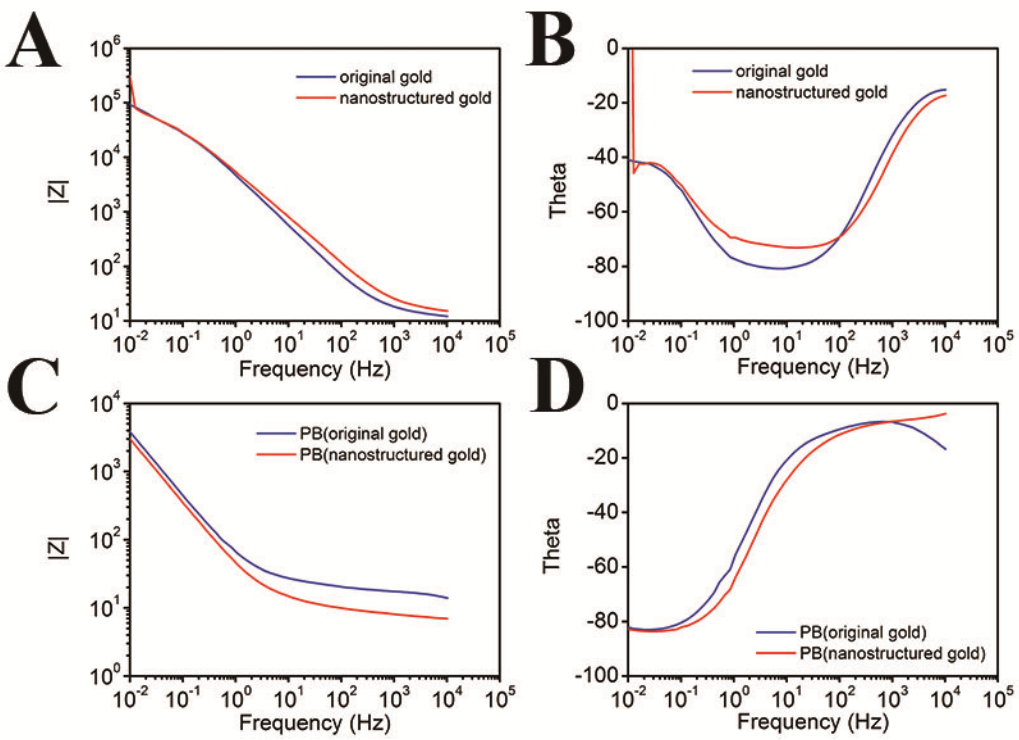

fig. S11. Bode plot of O-Au, N-Au, O-PB, and N-PB scan frequency of 1×10^{-2} to 1×10^{-4} Hz. (**A**) Impedance and (**B**) phase of O-Au and N-Au. (**C**) Impedance and (**D**) phase of O-PB and N-PB.

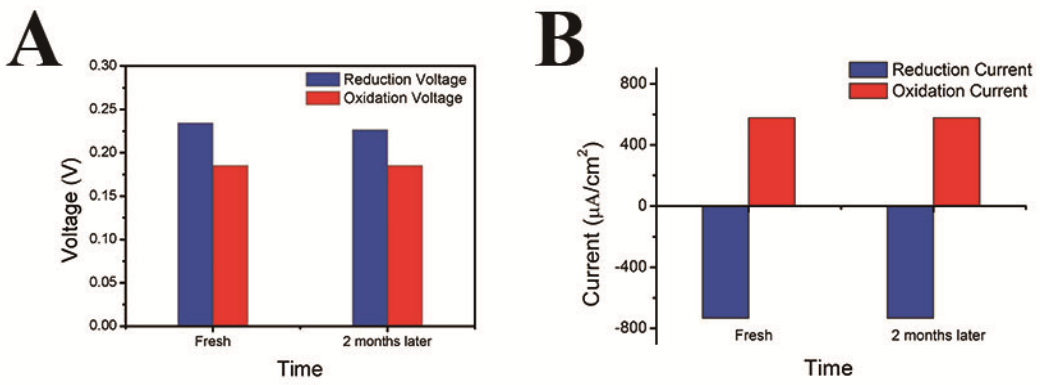

fig. S12. Electrochemical characterization of the N-PB after 2 months' storage. (**A**) CV redox peak voltage and (**B**) current change of N-PB after two months' storage.

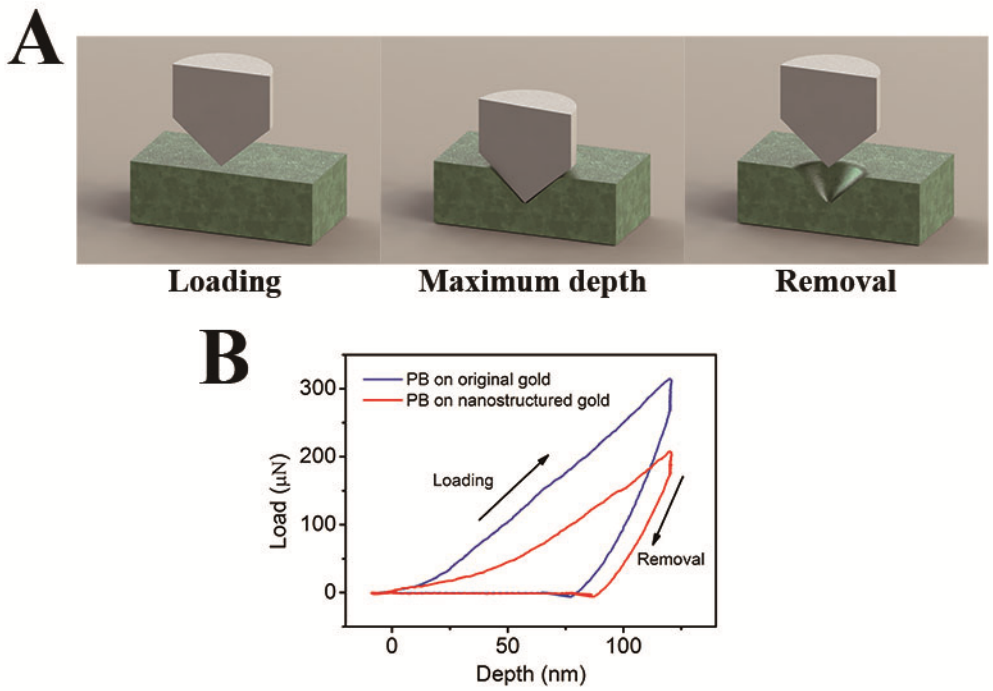

fig. S13. Mechanical property measurement of O-PB and N-PB. (**A**) Schematic of nano indenter measuring process. (**B**) Load-depth curve during loading and removing load.

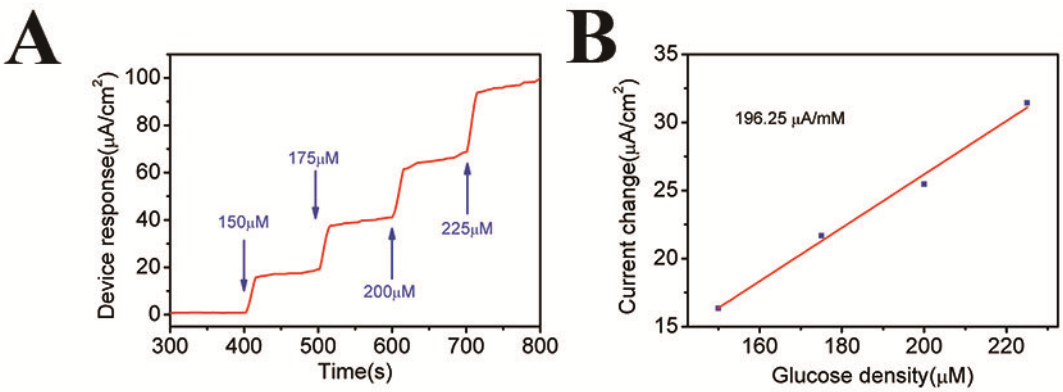

fig. S14. Biosensing device calibration experiment of high-density glucose. (**A**) I-t result of high density glucose (150μM-225μM at the rate of 25μM/step). (**B**) Device response and linear fitting result as a function of glucose density

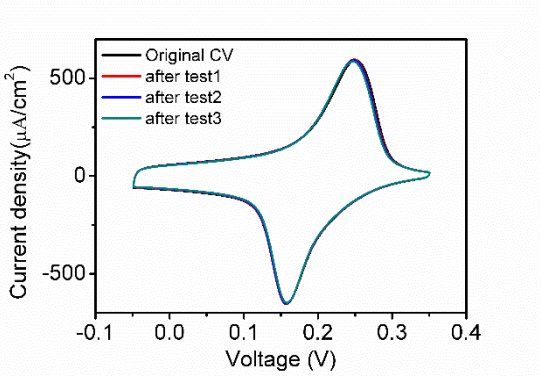

fig. S15. CV scan (−0.05 to 0.35 V versus reference electrode at a scan rate of 50 mV/s) of the device in four-time repeated glucose calibration experiments.

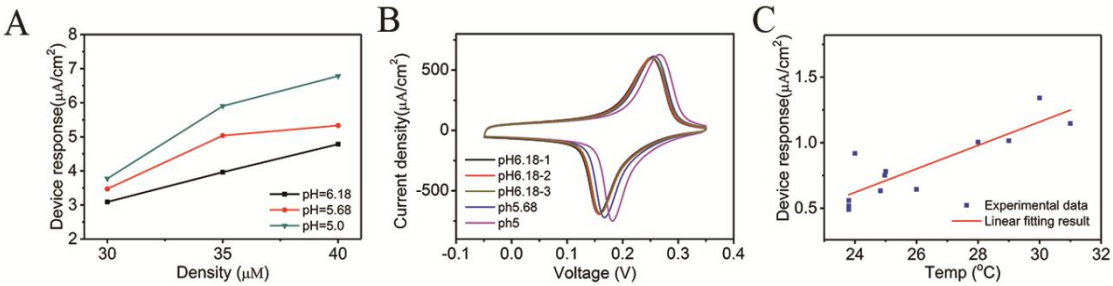

fig. S16. Influence of pH value and temperature change on device's performance. (**A**) Device's response to glucose at the different density (30μM -40μM at the rate of 5μM /step) in different pH value. (**B**) CV scan (-0.05V~0.35V v.s. reference electrode scan rate 50mV/s) in buffer solutions of different pH value. (**C**) Device response to the same density glucose under different solution temperatures.

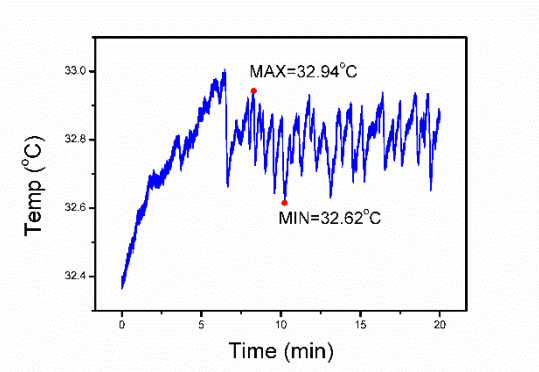

fig. S17. Skin surface temperature measurement in 20 min at room temperature with a Pt temperature sensor.

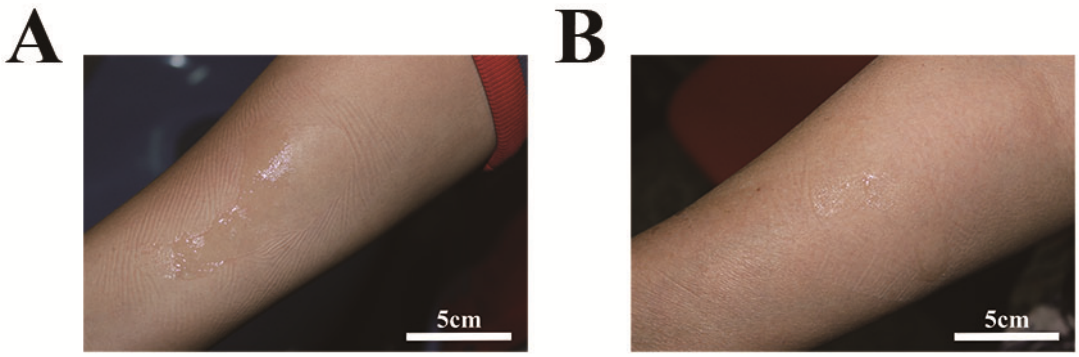

fig. S18. Skin surface condition. Skin surface condition after: (**A**) attaching paper battery for 20 min and (**B**) 4 times' electrochemical twin channel glucose measurements.

movie S1. ROSE transfer printing.